

# Interpretable Visual Question Answering by Reasoning on Dependency Trees

Qingxing Cao, Xiaodan Liang, Bailin Li and Liang Lin

**Abstract**—Collaborative reasoning for understanding each image-question pair is very critical but underexplored for an interpretable visual question answering system. Although very recent works also attempted to use explicit compositional processes to assemble multiple subtasks embedded in the questions, their models heavily rely on annotations or handcrafted rules to obtain valid reasoning processes, leading to either heavy workloads or poor performance on composition reasoning. In this paper, to better align image and language domains in diverse and unrestricted cases, we propose a novel neural network model that performs global reasoning on a dependency tree parsed from the question, and we thus phrase our model as parse-tree-guided reasoning network (PTGRN). This network consists of three collaborative modules: i) an attention module to exploit the local visual evidence for each word parsed from the question, ii) a gated residual composition module to compose the previously mined evidence, and iii) a parse-tree-guided propagation module to pass the mined evidence along the parse tree. Our PTGRN is thus capable of building an interpretable VQA system that gradually derives the image cues following a question-driven parse-tree reasoning route. Experiments on relational datasets demonstrate the superiority of our PTGRN over current state-of-the-art VQA methods, and the visualization results highlight the explainable capability of our reasoning system.

**Index Terms**—Visual Question Answering, Image and Language Parsing, Deep Reasoning, Attention Model

## 1 INTRODUCTION

THE task of visual question answering (VQA) is to predict the correct answer given an image and a textual question. The key to this task is the capability of coreasoning over both image and language domains. However, most of the previous methods [1], [2], [3] work in a manner similar to a black-box, i.e., simply mapping the visual content to the textual words by crafting neural networks. The main drawback of these methods is the lack of interpretability of the results, i.e., why are these answers produced? Moreover, it has been shown that the accuracy of these results may be achieved by overfitting the data bias in the VQA benchmark [4], and the absence of explicitly exploiting the structures of text and images leads to unsatisfactory performance on relational reasoning [5]. Very recently, a few pioneering works [6], [7], [8] have taken advantage of the structure inherently contained in text and images; these works parse the question-image input into a tree or graph layout and assemble local features of nodes to predict the answer. For example, the layout “*more(find(ball),find(yellow))*” means that the module should locate the ball and the yellow object in the image first and then combine the two results to determine whether there are more balls than yellow objects. However, these methods either rely on handcrafted rules for understanding questions or train a layout parser from scratch, which causes a large decrease in performance. We argue that these limitations severely limit their application potential for understanding general image-question pairs that may contain diverse and open-ended question styles.

To achieve a general and powerful reasoning system with the ability to enable reasoning over any dependency

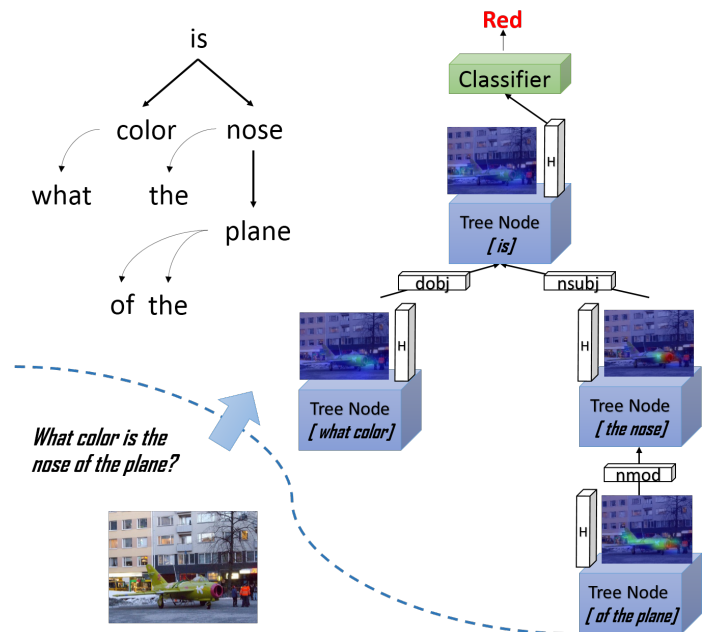


Fig. 1. Illustration of our parse-tree-guided reasoning network (PTGRN) that sequentially performs reasoning over a dependency tree parsed from the question. Conditioned on preceding word nodes, our PTGRN alternately mines visual evidence for nodes via an attention module and integrates the features of child nodes via a gated residual composition module.

parse trees of questions rather than fixed layouts as in prior works, we propose a novel parse-tree-guided reasoning network (PTGRN) that contains three collaborative modules to perform tailored reasoning operations for addressing the two most common word relations in the questions. As

- Q.Cao, X. Liang, B. Li and L. Lin are with the School of Data and Computer Science, Sun Yat-sen University, China
- Corresponding author: Xiaodan Liang (E-mail: xdliang328@gmail.com)

shown in Figure 1, given a specific dependency tree of a question parsed by an off-the-shelf parser, we construct a reasoning route that follows the parse tree layout, which is a tree structure composed of several types of nodes or edges. Our proposed network then alternately applies the three collaborative modules on each word node for global reasoning: 1) exploit local visual evidence of each word guided by the exploited regions of its child nodes, 2) integrate the messages of child nodes via gated residual composition, and 3) propagate the hidden and exploited map toward its parent with respect to the type of edges. Notably, in contrast to previous methods, our PTGRN is targeted toward a general and interpretable reasoning VQA framework that does not require any complicated handcrafted rules or ground-truth annotations to obtain a specific layout.

Specifically, we observe that the frequently used types of dependency relations can be categorized in two sets: whether the head is a predicate that describes the relation of its children (e.g.  $color \leftarrow is$ ,  $is \rightarrow nose$ ) or a word described by its child (e.g.  $furthest \rightarrow object$ ). We refer to the first set as a clausal predicate relation, which describes how a parent node composes its children, and we refer to the second as a modifier relation, which will help specify a object more concretely given the parent-child pairs. Thus, we design an attention module to unitize the information propagated from the modifier relations, a gated residual composition module to compose the messages from child nodes, and finally, a parse-tree-guided propagation module to transfer the node’s inner representations to its parent conditioned on the fine-grained relation types.

First, the attention module mines visual evidence from the image feature map given the word and encoded attention maps from child nodes. We sum the encoded attention maps from child nodes and fuse it with the image feature and word encoding. Then, we perform an attention operation on the fused hidden map to extract new local visual evidence for the current node. Second, two gated residual composition modules integrate both the mined local visual evidence and the attention map with the child nodes separately. To retain the information from an arbitrary number of child nodes, the module sums over the child nodes and learns a gate and a residual that will forget and update the hidden representations. Finally, the parse-tree-guided propagation module transforms the composed visual hidden representation and the attention hidden representation based on a head-dependent relation type and propagates the output message to the parent nodes. This edge-dependent module is capable of learning to encode how much of a hidden vector should be persevered given a specific head-dependent type. Thus, the gated residual composition module of parent nodes can forget a previous message if necessary. Finally, the hidden and attention output message of the root node will pass through a multilayer perceptron to predict the final answer.

A preliminary version of this work is published in CVPR2018. In this work, we inherit the idea of reasoning along the dependency parse tree, but we redevelop both modules such that it depends on specific types of relations rather than on a coarse-grained modifier relation and clausal predicate relation. Furthermore, to improve the performance on question types of “count” and “compare

number”, we compose and propagate the attention map the same as the hidden representations. These changes involve fewer manually designed structures and thus lead to better performance and generalization ability. We perform additional experiments to show the influence of the redeveloped components, and we evaluate the generalization ability with different tasks.

Extensive experiments show that our model can achieve state-of-the-art VQA performance on the CLEVR and FigureQA relational datasets. Moreover, the qualitative results further demonstrate the interpretability of our PTGRN on collaborative reasoning over image and language domains.

Our contributions are summarized as follows. 1) We present a general and interpretable reasoning VQA system that follows a general dependency layout composed of modifier relations and clausal predicate relations. 2) An attention module is proposed to enforce efficient visual evidence mining, a gated residual composition module is proposed for integrating knowledge of child nodes, and a parse-tree-guided propagation module is proposed to propagate knowledge along the dependency parse tree.

## 2 RELATED WORKS

*Visual question answering.* The VQA task requires coreasoning over both image and text to infer the correct answer.

The baseline method proposed in the VQA dataset [9] to solve this task uses a CNN-LSTM-based architecture, which consists of a CNN to extract image features and an LSTM to encode the question features. The method combines these two features to predict the final answer. In recent years, a large number of works have followed this pipeline and have achieved substantial improvements over the baseline model. Among these works, the attention mechanism [2], [10], [11], [12], [13], [14] and the joint embedding of image and question representation [3], [15], [16] have been widely studied. The attention mechanism learns to focus on the most discriminative subregion rather than the whole image, providing a certain extent of reasoning to the answer. Different attention methods, such as stacked attention [14] and coattention between question and image on different levels [2], constantly improve the performance of the VQA task. For the multimodal joint embedding, Fukui *et al.* [15], Kim *et al.* [3] and Hedi *et al.* [17] exploited the compact bilinear method to fuse the embedding of image and question and incorporated the attention mechanism to further improve the performance.

However, some recently proposed works [4], [18] have shown that the promising performance of these deep models might be achieved by exploiting the dataset bias. It is possible to perform equally well by memorizing the question-answer (QA) pairs or encoding the question with the bag-of-words method. To address this concern, newer datasets have recently been released. The VQAv2 dataset [4] was proposed to eliminate data biases through balancing QA pairs. The CLEVR [5] dataset consists of synthetic images, and it provides more complex questions that involve multiple objects. This dataset has also balanced the answer distribution to suppress data bias.

*Reasoning model.* Some prior works attempted to explicitly incorporate the knowledge into the network struc-

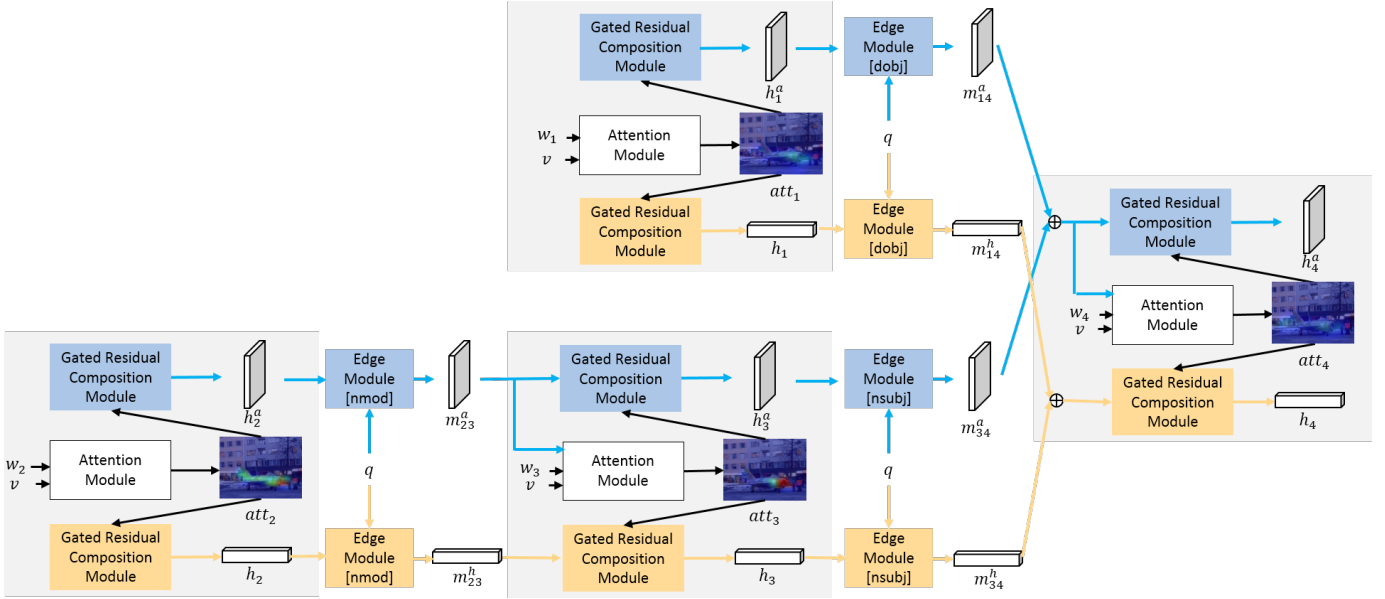


Fig. 2. The method pipeline of our PTGRN. Each PTGRN module is composed of an attention module and two gated residual composition modules. Each node receives the encoded attention map and the hidden features from its children, as well as the image feature and word encoding. The attention module is employed to generate a new attention map conditioned on image features, word encodings and previous attended regions given by the child nodes. The gated residual composition module is trained to evolve a higher-level representation by dropping and integrating features of its children with local visual evidence. The edge modules transform the output attention and hidden feature according to the question encoding and the relation types (*nmod*: *nominal modifier*, *dob*: *direct object* and *nsubj*: *nominal subject*). The blue arrows indicate the propagation process of attention map, and the yellow arrows represent the process of visual hidden representation.

ture. [19], [20] encoded both images and questions into discrete vectors, such as image attributes or database queries. These vectors enable their model to query external data sources for common knowledge and basic factual knowledge to answer questions. [21] actively acquired predefined types of evidence to obtain external information and predict the answer. Other recent works proposed networks to handle the composition reasoning. [22] augmented a differentiable memory and encoded long-term knowledge to infer the answer. The recently proposed neural reasoning network proposed to address compositional visual reasoning. Rather than using a fixed structure to predict the answer to every question, this line of work assembles a structure layout for different questions into predefined subtasks. Then, a set of neural modules is designed to solve a particular subtask. Some representative works [23], [24] generated their layouts based on dependency parsing. Later, [6], [7] used the sequence-to-sequence recurrent neural network (RNN) to predict the post-order of the layout tree and jointly trained the RNN and the neural module by using reinforcement learning or Expectation-Maximum approaches.

*Reasoning with Counting-like questions.* It is usually treated as a separated problem has been studied in VQA systems. Lempitsky and Zisserman [25] learned to produce a density map for counting. [26], [27] exploited a convolution network to estimate density and count the target objects. Zhang *et al.* [28] studied the problem of salient object subitizing, which recognizes the number of salient objects when only a few objects are present. Chattopadhyay *et al.* [29] further extended this approach by employing a divide and conquer strategy. They divided the image into subregions, counted within the regions individually, and

finally combined the results.

However, the counting problem has been less addressed in VQA. Anderson *et al.* [30] improved the “counting” question accuracy on VQAv2 [4] by first training an object detector on the Visual Genome dataset [31]. The pretrained detector was used to extract the objects from the VQAv2 dataset, and the attention operation was performed on candidate objects rather than the grid feature map only. Trott *et al.* [32] followed this pipeline, representing each image as a set of detected objects. Then, they treated the counting problem as a sequential decision process, deciding which candidate object should be counted at each step. Finally, they employed reinforcement learning to train the model. However, this pipeline is limited to the counting questions and cannot easily be migrated to answer other types of questions. Zhang *et al.* [33] reported that it is the soft attention mechanism that limits the counting capability of VQA models. Suppose that one should answer how many cats are in an image; then, cats counted by the normalized attention map will have weights sum to 1. Weighted sum pooling on these cats only results in a feature vector similar to a single cat. To resolve this problem, Zhang *et al.* [33] first generated an attention weight for each detected object; then, they performed “soft” non-maximum suppression on the weights to count the attended objects.

Inspired by these observations, we separately encode and propagate the mined visual evidence and attention map. The attention map at each node will be composed with its children’s output through a convolution GRU and will be propagated to its parent. We preserve the spatial feature of the attended region and utilize it to predict the counting questions.

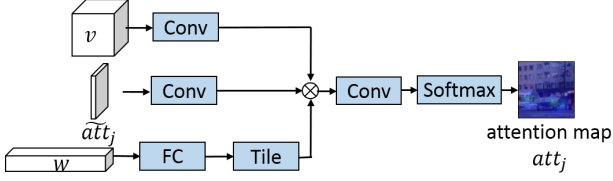


Fig. 3. The detailed architecture of the attention module. The image feature, previous attended regions and word encoding are project to 2048-d features. Then, they are fused by elementwise multiplication. Finally, the fused feature is projected to an 1-d attention map and normalized with softmax.

### 3 TREE-STRUCTURED COMPOSITION REASONING NETWORK

#### 3.1 Overview

Given free-form questions  $Q$  and images  $I$ , our proposed PTGRN model learns to predict the answers  $y$  and their corresponding explainable attention maps. We first generate the structure layout given the input question  $Q$  by parsing it into a tree structure using an off-the-shelf universal Stanford Parser [34]. To reduce the computational complexity, we prune the leaf nodes that are not nouns. Then, we perform VQA on it.

We denote the tree-structured layout as a 3-tuple  $G = (u, X, E)$ , where  $u = (v, q)$  contains the spatial feature  $v$  and question encoding  $q$ , which are global attributes for all nodes;  $X = \{(w_i, att_i, h_i)\}_{i=1:N^x}$  is the set of nodes in the parsed tree, where  $N^x$  is the number of nodes in the parse tree. Each node associates with words  $w_i$  in the origin question  $Q$  and will update its attended map  $att_i$  and hidden vector  $h_i$  during bottom-up inference.  $E = \{e_{i,j}\}_{i,j=1:N^x}$  is the set of edges in the parsed tree, and  $e_{i,j}$  represents the edge type between head node  $j$  and its dependent node  $i$  in the dependency parse tree.

Specifically, the spatial feature  $v$  is extracted from each image via any convolutional neural network pretrained on ImageNet (e.g. conv5 features from ResNet-152 [35] or conv4 features from ResNet-101 [35]). The word embedding vector  $w$  is obtained with a Bi-GRU [36]. Each word in the question is first embedded as a 200-dimensional vector, and then the words are feed into a bidirectional GRU. The final word embedding  $w$  is the hidden vector of the Bi-GRU at its corresponding position, and the hidden vector at the end of the question is extracted as question encoding  $q$ .

We update each node by post-order traversing on the tree. Each node  $j$  has several inputs: the image feature  $v$ , question encoding  $q$ , the word encoding  $w_j$ , and the message from its children  $\{m_{ij}\} = \{[m_{ij}^a, m_{ij}^h]\}$ . It generates its attention map  $att_j$  with the attention module  $f_a$ , and updates the hidden representation  $h_j$  and attention map encoding  $h_j^{att}$  with the gated residual composition module  $f_h$  and  $f_h^{att}$ . Finally, the parse-tree-guided propagation module  $f_e$  transfers the message  $[m_{jk}^a, m_{jk}^h]$  to its parent node  $k$  based on its attention map and hidden vector, as well as the edge  $e_{jk}$ , as shown in Figure 2.

#### 3.2 Attention Module

Specifically, as shown in Figure 3, the input attention feature  $att_j$  of each node  $j$  is first obtained by summing attention

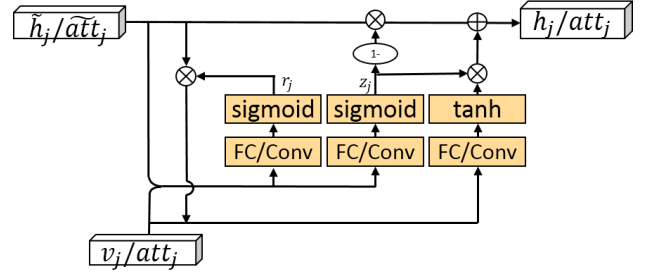


Fig. 4. The gated residual composition module utilizes the architecture of a gated recurrent unit to integrate the features of its children with local visual evidence or attention map. The sum of children input is considered as memory, and the local visual evidence or attention map is the input at the current step.

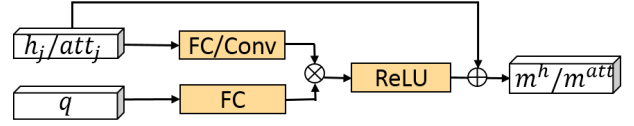


Fig. 5. The parse-tree-guided propagation module performs bilinear fusion between the hidden/attention map and question encoding. Different edge types have the same architecture but have different sets of weights.

features  $\{m_{ij}^a\}_{e_{i,j} \in E}$  of its child nodes  $\{i\}$ . Then, we project the spatial feature  $v$ , the input attention feature  $att_j$  and the word embedding  $w_j$  to a 2048-d space and perform elementwise multiplication on these three 2048-d features. Finally, the fused 2048-d feature is fed into another convolution layer, resulting in a new attention map  $att_j$ . We further apply softmax to regularize the resulting attention map into the range of  $[0, 1]$ . The visual representation  $v'_j$  of node  $j$  is then generated by the weighted sum of each grid feature in  $v$  given the attention weight  $att_j$ .

#### 3.3 Gated Residual Composition Module

In the preliminary work, the nodes only share weight at the same level, which contains many parameters and is not suitable for global reasoning with different parse trees. However, applying a single node module multiple times essentially acts as a recurrent network and will suffer from the gradient exploding/vanishing problems. Meanwhile, in the CLEVR dataset, there are a large number of objects referred to by their relations with other objects, such as “left of the big sphere” or “left of the brown metal”. To answer the question, the visual representation of “big sphere” is not necessary and might impact the final prediction. Previously, we dropped the hidden feature of these nodes when its head-dependent relation is a modifier relation. We want to enable the module to learn this drop process rather than using handcrafted rules. Here, we utilize the widely used gated recurrent unit to enable the module to learn the drop process.

As shown in Figure 4, the gated residual composition module  $f_h$  first sums the hidden features  $\{h_i\}$  of its children into  $\tilde{h}_j$ , and then it concatenates  $\tilde{h}_j$  with extracted local evidence  $v_j$ . Similar to a gated recurrent unit, the module generates the reset gate  $r_j$  and update gate  $z_j$  based on the concatenated hidden  $\tilde{h}_j$  and input  $v_j$ . Then, the module

produces an update vector  $c_j$ , and updates the hidden representation  $h_j$ :

$$\begin{aligned} \tilde{h}_j &= \sum_{(i,j) \in E} m_{ij}^h \\ z_j &= \sigma(W_z \cdot [\tilde{h}_j, v_j]) \\ r_j &= \sigma(W_r \cdot [\tilde{h}_j, v_j]) \\ c_j &= \tanh(W \cdot [r * \tilde{h}_j, v_j]) \\ h_j &= (1 - z) * \tilde{h}_j + z * c_j \end{aligned} \quad (1)$$

Compared with our preliminary work, which has  $c_j = \tanh(W \cdot [\tilde{h}_j, v_j])$  and  $h_j = \tilde{h}_j + c_j$ , we add an update gate and reset gate to the residual composition. These two gates can reduce the effect of the gradient exploding/vanishing problems when applying a single node multiple times and enable us to reuse the node module across multiple heights at the parse tree. The update process is also similar to that in Child-Sum Tree-LSTMs [37]. In [37], the LSTM cell calculates forget gates for each of the memories from its child, whereas we simplify this process by first summing over the children’s hidden representation and output a single reset and forget gate for updating the hidden  $h_j$ .

### 3.4 Parse-tree-guided propagation module

Rather than directly blocking the hidden representation or attention map based on two coarse-grained categories, namely, modifier relations and clausal predicate relations, we add a new module to transfer the hidden representation to its parent node based on the fine-grained dependency relation, as shown in Figure 5. For different types of edges, we apply the same module on hidden  $h_j$  but with different sets of weights. The module performs multimodal bilinear pooling on the hidden  $h_j$  and the question encoding  $q$ , and it generates the message for its parent  $m_{jk}^h$ . Specifically, fully connected layers are applied to project both the hidden representation  $h_j$  and question encoding  $q$  into two feature vectors that have the same size as  $h_j$ . Then, we perform elementwise multiplication on these two features, and we apply ReLU nonlinearity on the multiplied vector. Finally, we add it to  $h_j$ , resulting in hidden vector  $m_{jk}^h$  that will be passed through the edge.

$$m_{jk}^h = h_j + \text{ReLU}((W_{e_{jk}}^h \cdot h_j + b_{e_{jk}}^h) * (W_{e_{jk}}^q \cdot q + b_{e_{jk}}^q)) \quad (2)$$

where  $e_{jk}$  indicates the type of dependency relation between node  $j$  and its parent node  $k$ . There are a total of 22 relation types that reside in the dependency parse tree for questions in the CLEVR dataset; thus, we have  $e_{jk} \in [1, 22]$ .

### 3.5 Counting on attention map

The preliminary work did not perform well on “counting” questions. As reported by [33], the soft attention mechanism limits the ability of a model in “counting”. Suppose that there are two “small red metal spheres” in the image; their spatial features will be the same. The normalized soft attention map that has attended these two objects will assign each of them a weight of 0.5. After the weighted sum, the resulting feature is essentially the same as a single object in the image and has an attention weight of 1.

TABLE 1  
The two major categories of relations that appear in the universal dependencies.

Clausal Predicate Relation	Relation Description
NSUBJ	Nominal subject
NSUBJPASS	Passive nominal subject
CSUBJ	Clausal subject
CSUBJPASS	Clausal passive subject
DOBJ	Direct object
IOBJ	Indirect object
CCOMP	Clausal complement
XCOMP	Open clausal complement
Modifier Relation	Relation Description
NMOD	Nominal modifier
AMOD	Adjectival modifier
NUMMOD	Numeric modifier
ADVMOD	Adverbial modifier
APPOS	Appositional modifier
ACL	Clausal modifier of noun
DET	Determiner
CASE	Prepositions, postpositions
COMPOUND	Compound

To resolve these problems, in addition to propagating the attended feature  $h_j$  through the tree, we also encode the attention map  $att_j$  itself and pass it to the parent node. Specifically, the attention map  $att_j$  is composed with the message from its children  $\sum_{e_{ij} \in E} m_{ij}^a$  through convolution GRU. The output hidden  $h_j^{att}$  is then transformed to message  $m_{jk}^a$  to its parent node  $k$  based on the edge  $e_{jk}$ . The composition and propagation are similar to how our model composes and propagates hidden representation  $h$ , except we replace most of the fully connected layers with convolution layers.

### 3.6 The proposed PTGRN model

Given the tree-structured layout of the dependency tree, our PTGRN module is sequentially used on each word node to mine visual evidence and integrate features of its child nodes from bottom to top, and then it predicts the final answer at the root of the tree. Formally, each PTGRN module can be written as

$$\begin{aligned} att_j &= f_a(\{m_{ij}^a\}_{e_{ij} \in E}, v, w), \\ v_j &= att_j * v, \\ h_j &= f_h(\{m_{ij}^h\}_{e_{ij} \in E}, v_j), \\ h_j^{att} &= f_h^{att}(\{m_{ij}^a\}_{e_{ij} \in E}, att_j), \\ m_{jk}^h &= f_{e_{jk}}^h(h_j, q), \\ m_{jk}^a &= f_{e_{jk}}^a(h_j^{att}, q) \end{aligned} \quad (3)$$

We process each node by post-order traversing on the dependency tree. The type of edge indicates whether a node serves as a modifier, which can modify their parent node by referring to a more specific object, or is a subject/object of its predicate parent node. We thus pass both the attention map and hidden representation of a node to its parent based on the edge such that the parent node can generate a more precise attention map as  $att_j$  or integrate the features of child nodes to enhance the representation given the predicate word.

After propagating through all word nodes, the output message of the root node  $[m_{root}^h, m_{root}^a]$  are used to predict



the answer. We perform global max pooling on the encoded attention map  $m_{root}^a$  and concatenate it with  $m_{root}^h$ . This concatenated feature are passed through a multilayer perceptron with three layers to predict the final answer  $y$ .

Our model is stacked by a list of node module following a tree-structured layout. Weights are shared across all node modules. The entire model can be trained in an end-to-end manner with only the supervision signal  $y$ .

### 3.7 Head-dependent relations

A dependency-based parser draws directed edges from head words to dependent words in a sentence. It also labels the head-dependent relations to provide an approximation of the relationship between predicates and their arguments. One of the most widely used head-dependent relation sets is Universal Dependencies (UD) [38]. It has a total of 42 relations that can be clustered into 9 categories. However, the frequently used relations concentrate on only two of them: the core dependents of clausal predicate and the noun dependents. In this work, we make some small modifications to the noun dependent sets and refer to these two types of relationships as clausal predicate relation  $P$  and modifier relation  $M$ . The details of both sets are shown in Table 1.

Dependents of clausal predicate relation  $P$  describe syntactic roles with respect to a predicate that often describes how to compose its children. For example, in the question *What color is the nose of the plane?*, the word *is* is the head of *color* and *nose*, and their relations are  $(is, color) = direct\ object$  and  $(is, nose) = nominal\ subject$ . Thus, the word *is* tells us how to compose words *color* and *nose*, such as using a function “describes(*color*, *nose*)” in a modular network [23]. Thus, the composition module should learn to compose children’s hidden  $\{m^h\}$ , while children’s attention region  $\{m^a\}$  has less effect given clausal predicate relation  $P$ .

The modifier relation  $M$  categorizes the ways in which words can modify their parents. For example, the modifier relation  $M$  of the question *What size is the cylinder that is left of the brown metal thing* from the CLEVR dataset [5] can be the relation  $(left, brown\ metal\ thing) = nominal\ modifier$ . The reason is that the word *left* indicates the region related to *brown metal thing* rather than *cylinder*, which is similar to the “transform(*left*, *thing*)” relation in the modular network [23]. Thus, the attention map should be obtained for the parent node according to attention maps  $\{m^a\}$  of its children, and the composition module should consider less of children’s hidden  $\{m^h\}$  if the edge belongs to modifier relation  $M$ .

Therefore, our parse-tree-guided propagation module will learn to transfer and drop the knowledge given the fine-grained edge types, and the gated residual composition module learns how much of the current mined knowledge will be used to compose and update messages  $\{m^a\}$  and  $\{m^h\}$ .

## 4 EXPERIMENT

We validate the effectiveness and interpretation capability of our models on synthetic datasets (i.e., CLEVR and Sort-of-CLEVR) that mainly focus on relation reasoning.

### 4.1 Datasets

CLEVR [5] is a synthesized dataset with 100,000 images and 853,554 questions. The images are photorealistic rendered images with objects of random shapes, colors, materials and sizes. The questions are generated using sets of functional programs, which consist of functions that can filter certain colors and shapes or compare two objects. Thus, the reasoning routes required to answer each question can be precisely determined by the underlying function program. Unlike natural image datasets, this dataset requires a model capable of reasoning on relations to answer the questions.

FigureQA [39] is also a synthesized dataset. This dataset contains 100,000 images and 1,327,368 questions for training. In contrast to CLEVR, the images are scientific-style figures. The dataset includes five classes: line plots, dot-line plots, vertical and horizontal bar graphs, and pie charts. The questions also concern various relationships between elements in the figures, such as the maximum, area under the curve, intersection and so on. Thus, this dataset also requires the VQA model to perform relational reasoning on the plot elements.

Sort-of-CLEVR [40] consists of synthesized images of 2D colored shapes. Each image has exactly 6 objects that can be unambiguously identified by 6 colors, and the objects have random shapes (square or circle) and positions. Each image is associated with 20 questions asking about the shape or position of a certain object, 10 of which are nonrelational questions that query the object by its unambiguous colors, and the other 10 are relational questions that query the object with the furthest or closest relation to another unambiguous colored object. This dataset is visually simpler than CLEVR, but it also requires a model that is capable of relational reasoning. Since the original dataset is not available, we generate a set following their detailed description, including 9800 images for training and 200 for testing.

### 4.2 Implementation details

For the CLEVR dataset, we employ the same settings used in [5], [41] to extract the image feature and word encoding. We first resize all images to  $224 \times 224$ , and then we extract the conv4 feature from ResNet-101 pretrained on ImageNet. The resulting  $1024 \times 14 \times 14$  feature maps are concatenated with a 2-channel coordinate map. It is further fed into a single  $3 \times 3$  convolution layer. The resulting  $128 \times 14 \times 14$  feature maps are also concatenated with the 2-channel coordinate map and then passed through our PTGRN. We encode the questions using a bidirectional GRU with 512-d hidden states for both directions. The hidden vector of Bi-GRU at the corresponding word position is extracted to be this word’s encoding  $w$ . The hidden representations of gated residual composition modules are 128-d for both  $h_j$  and  $h_j^{att}$ . The messages generated by parse-tree-guided propagation module modules are also 128-d for both attention map and hidden representation. The three-layer MLP has output sizes of 512, 1024 and 29, where 29 is the number of candidate answers.

We resize the images in Sort-of-CLEVR to  $128 \times 128$ , and then we use a four-layer CNN, where each layer has a  $3 \times 3$  kernel and 24-channel output, to extract the image features. The resulting feature maps are concatenated with

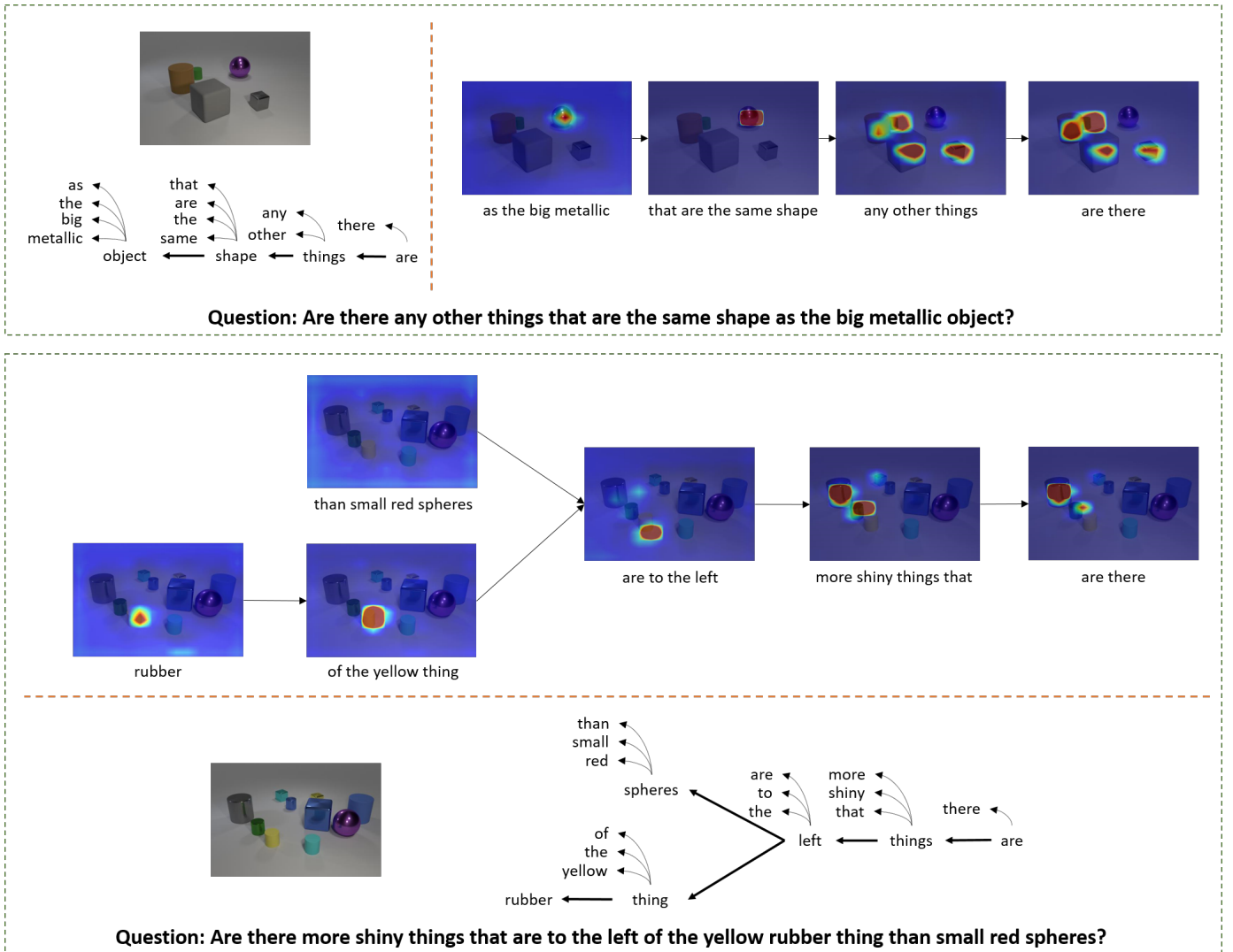


Fig. 6. Two examples of the dependency trees of questions and corresponding regions attended by our model at each step on the CLEVR dataset. The questions are shown on the bottom. The input images and dependency parse trees are shown on the left and lower part. The arrows in the dependency tree are drawn from the head words to the dependent words. The curved arrows point to the pruned leaf words that are not a noun. Thus word “are” is the root node for both examples.

TABLE 2

Comparisons of question answering accuracy on the CLEVR dataset. The performances of question types *Exist*, *Count*, *Compare Integer*, *Query*, and *Compare* are reported in each column. LBP-SIG [41] and RN [40] only report the total accuracy of question types *Compare Integer*, *Query*, and *Compare*, and their performances on these types are merged.

Method	Exist	Count	Compare Integer			Query				Compare				Overall
			Equal	Less	More	Size	Color	Material	Shape	Size	Color	Material	Shape	
LBP-SIG [41]	79.63	61.27	80.69			88.59				76.28				78.04
RN [40]	97.8	90.1	93.6			97.9				97.1				95.5
N2NMN scratch [6]	72.7	55.1	71.6	85.1	79.0	88.1	74.0	86.6	84.1	50.1	53.9	48.6	51.1	69.0
N2NMN cloning expert [6]	83.3	63.3	68.2	87.2	85.4	90.5	80.2	88.9	88.3	89.4	52.5	85.4	86.7	78.9
N2NMN policy search [6]	85.7	68.5	73.8	89.7	87.7	93.1	84.8	91.5	90.6	92.6	82.8	89.6	90.0	83.7
PE-semi-9K [7]	89.7	79.7	85.2	76.1	77.9	94.8	93.3	93.1	89.3	97.8	94.5	96.6	95.1	88.6
PE-Strong [7]	97.7	92.7	98.0	99.0	98.9	98.8	98.4	98.1	97.3	99.8	98.5	98.9	98.4	96.9
ACMN	94.21	81.37	75.06	88.23	81.51	92.61	86.45	92.35	90.65	98.50	97.44	94.93	97.37	89.31
Ours	97.85	91.75	93.00	95.65	96.89	95.90	94.32	95.50	96.25	99.27	98.14	98.33	98.13	95.47

the 2-d coordination map. Thus, the input spatial features have a size of  $26 \times 8 \times 8$ , and all of the gated residual composition modules and propagation modules also output 128-d features. The words in a question are first embedded as a 300-d vector, and then the entire question is encoded by a bidirectional LSTM [42], which has 150-d hidden units

in both directions. The word encoding vector is represented by the LSTM hidden vector at its corresponding position.

We resize the images in FigureQA to  $256 \times 256$ . Then, we use a five-layer CNN to extract the image features. Each layer has a  $3 \times 3$  kernel and stride of 2. The dimensions of the feature map in first four layers are 64, and the last

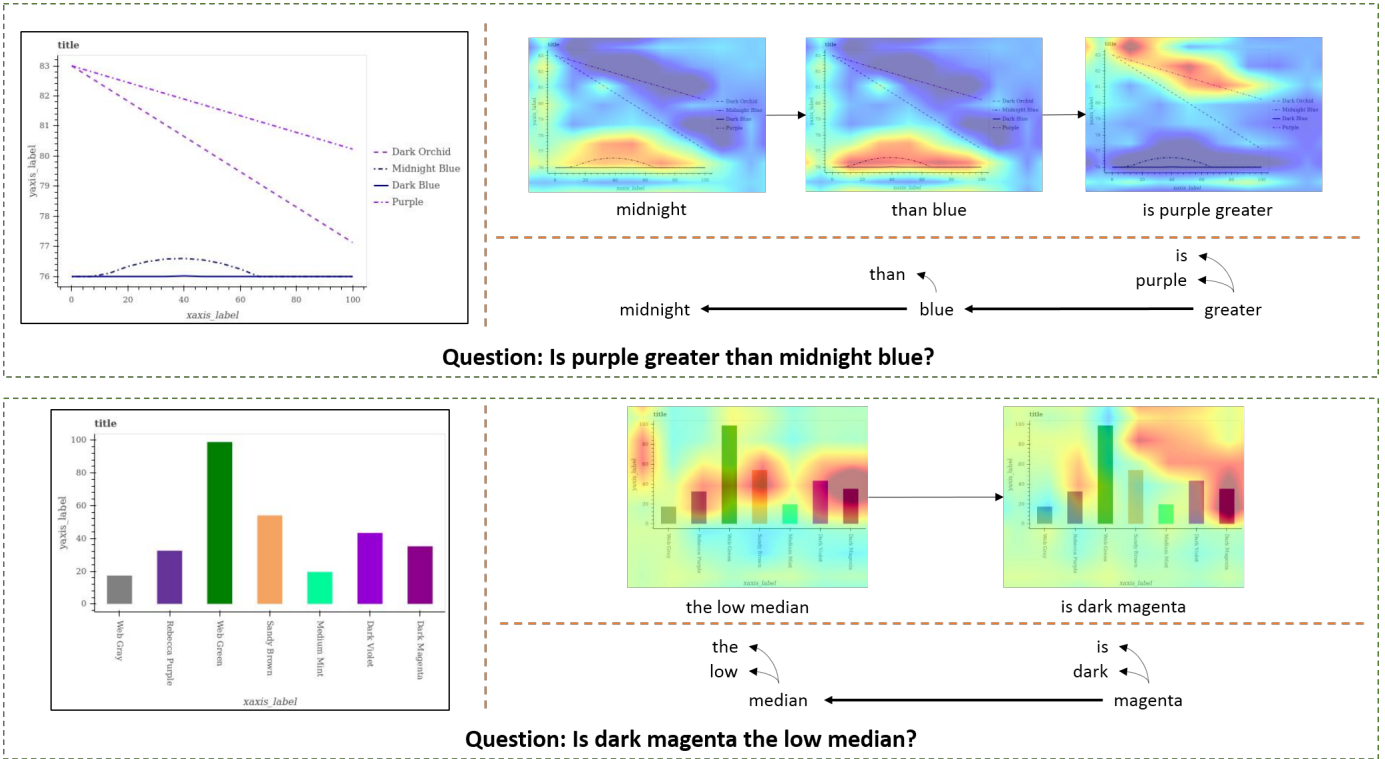


Fig. 7. Two examples of the dependency trees of questions and corresponding regions attended by our model at each step on the FigureQA dataset.

TABLE 3

Comparisons of question answering accuracy on FigureQA validation and test sets that have alternative color scheme.

Model	Val	Test
Text only	50.01	50.01
CNN+LSTM	56.16	56.00
CNN+LSTM on VGG-16 features	52.31	52.47
RN	72.54	72.40
Ours	86.25	86.23

layer has 128-channel outputs. The resulting feature map is concatenated with the 2-d coordination map. Thus, the spatial feature map has a size of  $130 \times 8 \times 8$ . The output hidden representations of gated residual composition modules and propagation modules are 128-d. The words in a question are first embedded as a 200-d vector, and then the whole question is encoded by a bidirectional GRU, which has 1024-d hidden units in both directions. The word encoding vector is represented by the GRU hidden vector at its corresponding position.

For all three of these datasets, we train our model on the training split, and then we evaluate on the validation and test split. The model is trained with the Adam optimizer [43]. The base learning rate is 0.0003 for CLEVR, and it is 0.0001 for FigureQA and Sort-of-CLEVR. The batch size is 64. The weight decay,  $\beta_1$  and  $\beta_2$  are 0.00001, 0.9, and 0.999, respectively.

### 4.3 Comparison with State-of-the-art

#### 4.3.1 CLEVR dataset

Table 2 shows the performances of different works on the CLEVR test set. The previous end-to-end modular net-

work [6] and program execution engine [7] are referred to as N2NMN and PE, respectively. Both of these approaches use the functional programs as the ground-truth layout, and they train their question parser in a sequence-to-sequence manner with strong supervision. They also have variants that are trained using semisupervision or no supervision signals. “N2NMN scratch” indicating the end-to-end modular network without layout supervision and “N2NMN cloning expert” show the results of their models trained with full supervision. “N2NMN policy search” provides this model’s best results if it further trains the parser from “N2NMN cloning expert” with RL. As shown, our model outperforms all of these previous models by a large margin without using any dataset-specific layout, thus showing the good generalization capability of our PTGRN. Our PTGRN also surpasses the program execution engine [7] variant trained with semisupervision (as “PE-semi-9K”).

“ACMN” shows the results of our preliminary work. It also performs structured reasoning along the dependency tree, but it has three differences. 1) Rather than learning a forget gate, it drops the attention map or hidden representation according to whether the edge belongs to clausal predicate relation or modifier relation. 2) It performs fusion between hidden and question encodings independent of the edge types, but each node only shares weights with other nodes at the same height. 3) It propagates the attention map without extra encoding, and the attention module will mask the spatial feature adversary based on the children’s attention maps. As shown, our proposed modules significantly improve the performance by 6.29%. Furthermore, PE-Strong [7] used all program layouts as additional supervision signals, and RN [40] is a black-box model



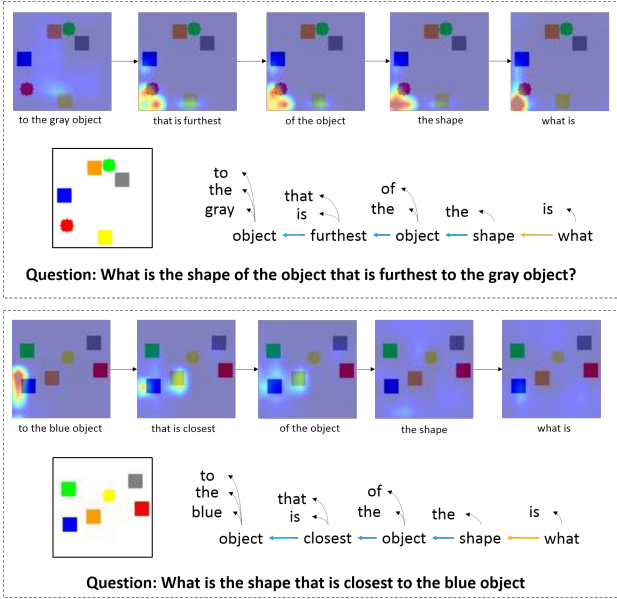


Fig. 8. Examples of parse trees and corresponding regions attended by our PTGRN on the Sort-of-CLEVR dataset.

TABLE 4  
Sort-of-CLEVR results by competing methods and variants of our model.

	Nonrelational	Relational
Ours-w/o residual	99.15	94.70
Ours-w/o gate	99.70	96.70
Ours-relocate [6]	97.95	83.75
Ours-concat	98.70	89.15
CNN+MLP [40]	-	63
CNN+RN [40]	-	94.0
ACMN	<b>99.85</b>	96.20
Ours	99.80	<b>97.55</b>

that lacks interpretability. Our PTGRN not only obtains results comparable with program execution engine [7] with full supervision (as “PE-Strong”) and relation network (as “RN”) [40] but also provides more explicit reasoning results without dataset-specific layout supervision.

Figure 6 shows the promising intermediate reasoning results achieved by our PTGRN. The images and the dependency parse trees are shown on the left and bottom. The attention map that our model obtained at each tree node is displayed on the right and top. The first example shows that our model can first locate the “big metallic object”, while the phrase “same shape” attends the same region. Later, our model attends all objects except the metallic object given the phrase “any other things”, and the phrase “are there” extracts the attended objects’ feature and predicts the answer “no”. The second example first locates the “yellow rubber” thing, and it attends nothing given the phrase “small red spheres” because there is no such object in the image. Then, it sequentially attends the “left” and “shiny things” based on the yellow rubber object and predicts the answer “yes” in the end.

TABLE 5

Comparisons of question answering accuracy on the CLEVR-CoGenT validation set. Each method is trained on condition A only, and is evaluated on both condition A and B.

Model	Train A	
	A	B
CNN+LSTM+SA	80.3	68.7
PG+EE (18K prog.)	96.6	73.7
CNN+GRU+FiLM	98.3	75.6
CNN+GRU+FiLM 0-Shot	98.3	78.8
Ours	97.35	83.50

#### 4.3.2 FigureQA dataset

Table 3 presents the comparisons among our model and prior works on the FigureQA dataset. The baseline methods “Text only”, “CNN+LSTM”, “CNN+LSTM on VGG-16 features” and “RN [40]” were originally reported in [39]. As shown, our PTGRN outperforms all baseline methods by a large margin, including the relational network, which has achieved great performance on the CLEVR dataset. This result demonstrates the generalization ability of our model across different datasets.

Figure 7 shows the reasoning route on the FigureQA dataset. The first question queries whether the plot of purple is greater than midnight blue. Our model successfully locates midnight blue in the first two steps, and then it locates the dotted purple line and predicts the answer. The second example first locates several bars that are “median”, and then it attends the “dark magenta” bar to predict that it is the low median.

#### 4.3.3 Sort-of-CLEVR dataset

Table 4 shows the comparisons among our model, its variants and prior works on the Sort-of-CLEVR dataset. As described in [40], since the visual elements in this dataset are quite simple, a simple CNN+MLP baseline model can achieve over 94% accuracy for nonrelational questions but fails for relational questions. We thus mainly focus on comparing the results for relational questions. The results of two baselines (i.e., “CNN+MLP [40]” and “CNN+RN [40]”) were originally reported in [40]. The actual accuracy values for nonrelational questions are not reported since both models achieve nearly 100% accuracy. As shown, our PTGRN achieves superior results over the two previous methods for answering relational questions requiring the model to have a strong capability in relation reasoning rather than overfitting the dataset bias as in previous works.

Figure 8 shows the resulting attention regions following the general dependency tree for the questions achieved by our PTGRN, which clearly demonstrates its interpretability. The first example locates the region that is “furthest” to the “gray object”. Our model successfully attends the correct objects in the last few steps to answer the question. The second example first attends the “blue object”. Then, it shift its attended region to the “closest” area. Finally, our model correctly locates the orange rectangle object to answer the question.

#### 4.4 CLEVR Composition Generalization Test

The CLEVR composition generalization test (CLEVR-CoGenT) [5] was proposed to investigate the composition

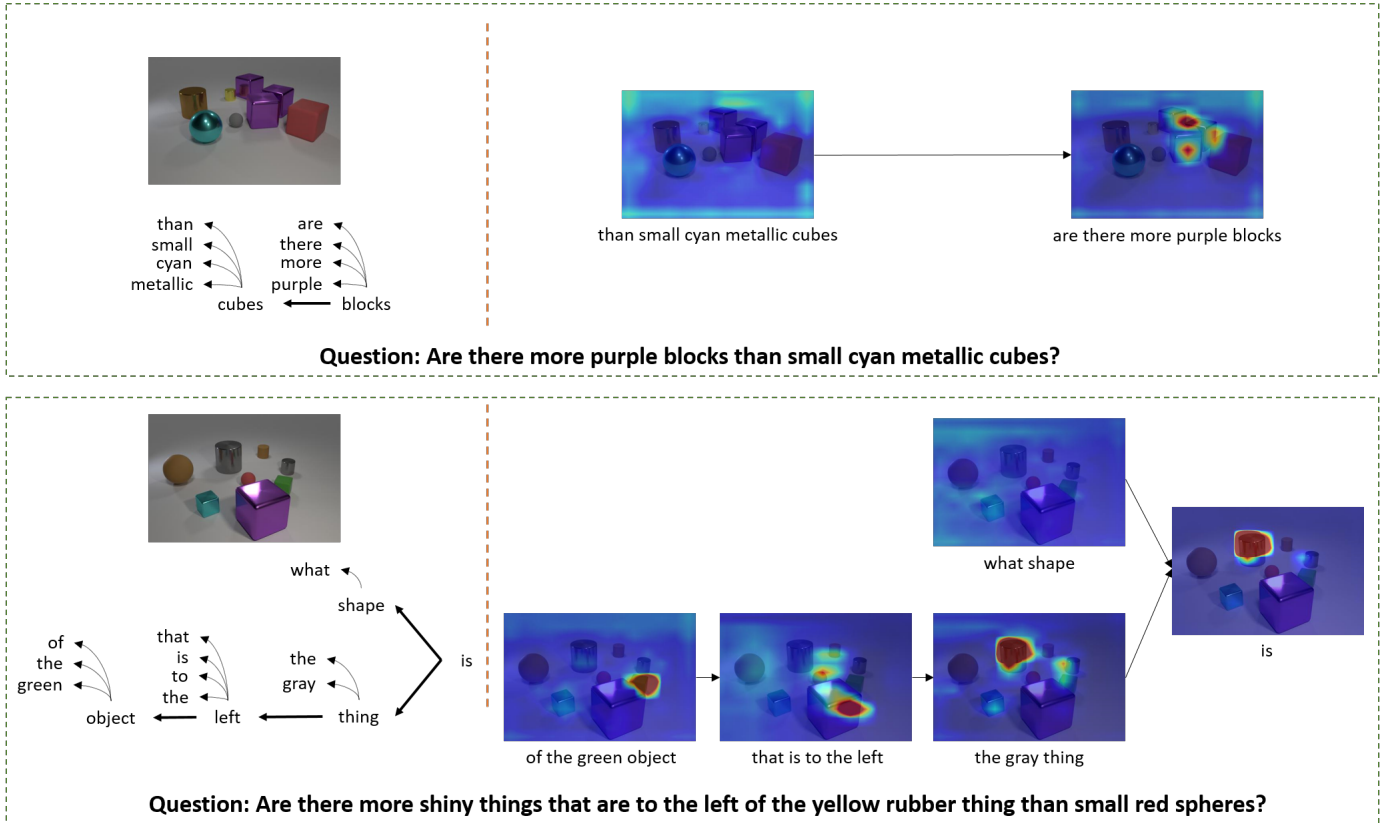


Fig. 9. Two examples of the dependency trees of questions and corresponding regions attended by our model at each step on the CLEVR-CoGen test set.

generalization ability of a VQA model. This dataset contains synthesized images and questions similar to CLEVR, but it has two conditions: in condition A, all cubes are gray, blue, brown, or yellow, and all cylinders are red, green, purple, or cyan. In condition B, cubes and cylinders swap color palettes. Thus, one model cannot achieve good performance on condition B by simply memorizing and overfitting the samples in condition A.

We report the accuracy of our model in Table 5. “Ours” represents the model that we trained on the CLEVR dataset with the same settings and hyperparameters. We train it on training set that has condition A, and evaluate it on validation set that has both condition A and B. Our model achieves 97.35% accuracy on condition A, and it obtains 83.50% accuracy on condition B without fine-tuning on the alternative color scheme set B. Our method achieves higher accuracy on condition B while the accuracy on condition A is similar to PE [7] and FiLM [44]. This result demonstrates that our model has better composition generalization ability.

In Figure 9, we show our model’s reasoning routes on the CLEVR-CoGenT condition B validation set. We display the image and parse tree on the left, and the attention map at each step is shown on the right. The first questions query the number between purple blocks and the cyan metallic cubes. When there are no “cyan metallic cubes”, the first step attends nothing. At the second step, it successfully attends the three purple blocks. Note that there is no purple block in the training set, and our model correctly distinguishes the purple blocks from the red block. The second example

follows the parsed tree and successively attends the “green object”, its “left” and the “gray thing”. Gray cylinders are also not present in the training set, and our model can locate the color “gray” and then predict the answer. These examples show that our model can locate the color and the object separately and that it possesses composition generalization ability to a certain extent.

#### 4.5 Ablation Studies

##### 4.5.1 CLEVR dataset

We first compare the performance with and without the redeveloped components in our model. We incrementally added the modules to the baseline model, and we show the accuracy on the CLEVR validation set in Table 6.

**Baseline model** Baseline results are obtained with the adversarial composition modular network (ACMN) presented in the preliminary work. The ACMN performs structured reasoning along a general dependency parse tree. In each node, it 1) first mines local visual evidence with the adversarial attention module: the spatial feature is masked by  $ReLU(1 - att)$ , where  $att$  is the sum of children’s attention map; then, the masked spatial feature is fused with word embeddings and convolved to a 1-d attention map  $att$ . 2) Then, compose the attended local visual feature  $v$  with the sum of children’s hidden representation  $\tilde{h}$ : it generates the residual by applying a fully connected layer on concatenated  $[v, \tilde{h}]$ ; then, adds the residual to  $\tilde{h}$ , fuses it with question encoding and results in the current hidden  $h$ . 3) Finally, it propagates the attention map  $att$  to its parent

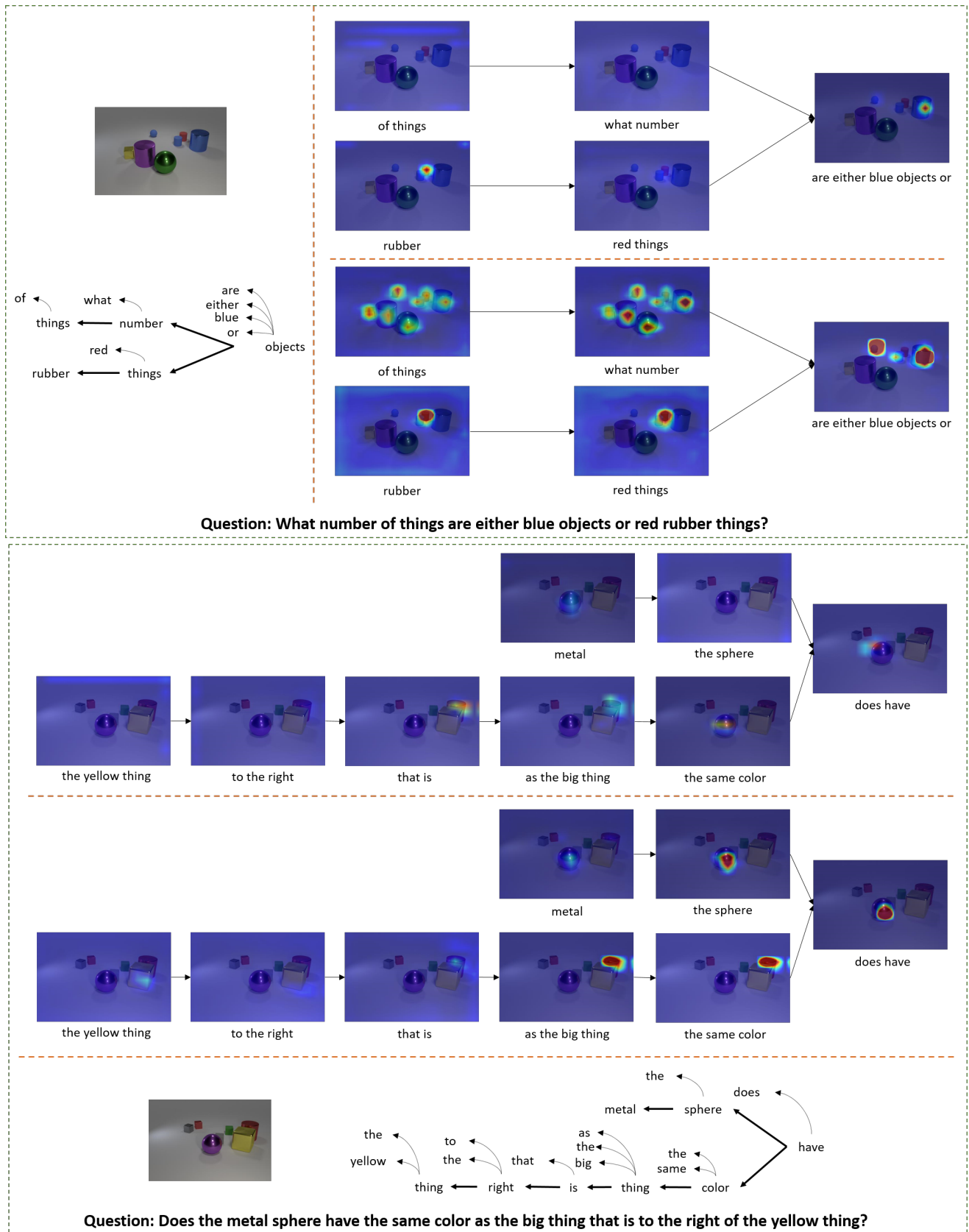


Fig. 10. Quality comparison between the model with and without the GRU and propagation module

TABLE 6

CLEVR validation accuracy for ablations. We incrementally replace the components of baseline model with redeveloped modules, and report their results on each row.

Method	Exist Count		Compare Integer			Query				Compare			Overall	
			Equal	Less	More	Size	Color	Material	Shape	Size	Color	Material		Shape
baseline	94.20	80.46	74.21	88.98	83.62	93.10	86.42	92.16	89.72	97.17	96.54	95.94	96.64	89.01
+Edge	93.98	80.18	72.18	87.55	84.86	93.37	86.61	92.35	90.36	98.92	98.01	98.20	97.72	89.28
+Edge+GRU	95.23	82.62	83.93	92.04	91.89	92.61	85.92	92.23	89.44	98.56	98.37	97.88	97.69	90.44
+Edge+ConcatAtt	96.38	85.51	86.28	95.37	93.81	95.99	95.22	95.37	94.48	98.74	97.59	98.12	97.66	93.36
+Edge+GRU+ConcatAtt	95.81	86.31	85.44	94.90	93.13	96.03	96.12	95.58	94.06	98.72	98.32	98.23	97.88	93.53
+Edge+GRU+GRUAtt	96.80	87.50	89.00	96.04	95.33	96.76	96.18	96.31	95.11	99.39	98.76	98.27	98.03	94.42
+Edge+GRU+ConvGRUAtt	97.83	91.78	92.08	96.00	96.46	95.90	94.00	95.46	96.15	99.30	98.32	98.52	98.19	95.42

if the edge type belongs to modifier relation, or propagates the hidden  $h$  if the edge is a clausal predicate relation. Each node will share weights with other nodes at the same height.

To perform ablation studies on our PTGRN, we replace each module with our proposed components and evaluate them incrementally.

**Edge-dependent propagation** Compared with the baseline model, “+Edge” has the following changes: 1) each node now shares its weights with other nodes across different heights in the parsed tree; 2) the adversarial attention module is replaced by the proposed one described in section 3.2; and 3) it performs extra edge-dependent feature transformations between children and parents. These changes increase the performance by 0.27% and make the model easier to apply on different datasets without adjusting the maximum tree height. Moreover, it is more reasonable to reuse the same module to perform the same tasks.

**Gated residual** We investigate the effect of the gated residual module by comparing the accuracy with the “+Edge” model. The “+Edge” model composes the mined visual evidence  $v_j$  and its children nodes’ message  $\tilde{h}$  by concatenating them and performing a linear transform with a fully connected layer, while the “+Edge+GRU” model replaces it with a GRU, where  $v_j$  corresponds to the current input, and the message is the memory. Adding a GRU improves the accuracy by 1.16%. This result suggests that the GRU module has stabilized the recurrent process and improved the performance. If the attention map is encoded into a hidden representation, then whether the incoming message is gated has less performance effect. With the forget gate, the accuracy increases from 93.36% to 93.53%, as shown in “+Edge+ConcatAtt” and “+Edge+GRU+ConcatAtt”.

**Attention map encoding** There are multiple methods for encoding the attention map as a hidden representation. We evaluate several methods and report their answering accuracy in Table 6.

The first method is to flatten the attention map, apply a linear layer, and concatenate the resulting vector to hidden and propagate it to the parent. In the case of the CLEVR dataset, the  $14 * 14$  attention map  $att_j$  is flattened to a 196-d vector and projected to 128-d feature  $h_j^{att}$  with two fully connected layers. Then, it is concatenated with the mined visual evidence  $v_j$ . The accuracies are reported as “+Edge+ConcatAtt” and “+Edge+GRU+ConcatAtt”, where the first one composes the current hidden  $[v_j, h_j^{att}]$  and input hidden  $\tilde{h}$  by concatenating them, as in the preliminary work. In “+Edge+GRU+ConcatAtt”, we compose the  $[v_j, h_j^{att}]$  and  $\tilde{h}$  with a GRU-unit, as described in section 3.3.

Both methods pass the original attention map  $att_j$  to its parent. “+Edge+ConcatAtt” achieves 93.36% overall accuracy. “+Edge+GRU+ConcatAtt” achieves 93.53%, which is slightly higher than the 93.36% obtained by the model without GRU. From the accuracy per question type, we observe that “+Edge+ConcatAtt” performs slightly better on “compare integer” questions. These results indicate that updates the encoded attention map and hidden representation together will harm the counting ability of our model.

The second method is to investigate the influence of the separated modules for the attention map. We perform the experiment denoted as “+Edge+GRU+GRUAtt”. This method also first flattens the attention map to 196-d vector. Then, this vector is used to update the input attention feature  $\tilde{att}_j$  with another GRU rather than concatenating it with mined visual evidence  $v_j$ . The output hidden representation of the GRU  $h_j^{att}$  will be propagated to its parent node  $k$  based on the edge  $e_{jk}$ . Finally, the encoded attention map to the root node  $m_{root}^a$  will be concatenated with the hidden  $m_{root}^h$  and fed into the classifier to predict the answer. It achieves 94.42% overall accuracy on the validation set, which improves the accuracy of the “+Edge+GRU+ConcatAtt” baseline by 0.89%. This illustrates that it is necessary to process the attention map and hidden representation with different weights. This result is also consistent with our preliminary model, which processes the attention map and the hidden representation differently based on whether the edge is a modifier relation or clausal predicate relation.

The last approach is our full model, which is reported as “+Edge+GRU+ConvGRUAtt”. Compared with the second one, this approach utilizes the convolution GRU to preserve spatial information and propagate feature maps across the tree. We perform global max pooling on the feature map  $m_{root}^a$ , and concatenate it with the hidden representation to predict the final answer. It gains 1% over the second approach on the validation set. It is shown that preserving spatial information will lead to better performance.

**Quality comparison** We further compare the reasoning results generated by ACMN and PTGRN in Figure 10. The upper part shows the heat map given by ACMN, and the lower part displays the results of PTGRN. The first question queries the number of specific objects. ACMN correctly attends the “red rubber” things, but it only locates one of the blue objects; PTGRN has also found the “red rubber” and locates all of the objects given the phrases “of things” and “what number”. Finally, our PTGRN attends all three blue objects at the last step. The second example illustrates the process of locating the “big thing” and the “metal sphere”.

TABLE 7  
Accuracy on CLEVR with randomly perturbed dependency trees

Percentage of perturb	0	10%	30%	50%	70%
Accuracy	95.42	86.77	69.88	54.21	40.11

Although both models mined the corresponding objects at each step, PTGRN has higher confidences on its decision.

#### 4.5.2 Sort-of-CLEVR dataset

We then evaluate the variants of the composition module and attention module on the Sort-of-CLEVR dataset. The results are shown in Table 4.

**Parent-child composition** We first try removing both the residual connection and gate in our gated residual composition module. This variant, denoted as “Ours-w/o residual”, updates the hidden by applying a fully connected layer on the concatenated visual and children input  $[v_j, \tilde{h}]$ . Its accuracy decreases 2.85% on relational question answering by comparing with “Ours”. Furthermore, we keep the residual connection but remove the update gate in GRU, resulting in a variant “Ours-w/o gate”. It adds the update vector to the hidden  $\tilde{h}$  with the same scale of 1, and achieves 96.70% accuracy. Both variants perform worse than our full model, demonstrating the effectiveness of our gated residual composition module.

**Word attention** We also evaluate the results of other attention modules to demonstrate the effectiveness of our attention module. One commonly used attention module is the relocate module used in [6], resulting in our variant “Ours-relocate”. Another option for the attention module is to directly concatenate image features with the input attention maps *att* rather than performing elementwise multiplication, which is “Ours-concat”. The proposed attention module is demonstrated to obtain better question answering performance over these two attention alternatives.

#### 4.6 Perturbed tree-structure

Since our model relies on the parsed results of the parser, we perform experiments to investigate the impact of incorrectly parsed trees. We randomly distort the generated dependency trees and observe its effect on the final prediction. Specifically, for each dependency relation, we randomly perturb it with a certain probability by replacing its parent node and relation edge with a word randomly chosen from the sentence and possible relations, respectively. The results are listed in Table 7. As shown, the performance dramatically decreases as the number of perturbed relations increases. This result indicates that the parsing results are crucial to the performance.

## 5 CONCLUSION

In this paper, we propose a novel parse-tree-guided reasoning network (PTGRN) equipped with an attention module, a gated residual composition module, and a parse-tree-guided propagation module. In contrast to previous works that rely on annotations or handcrafted rules to obtain valid layouts, our PTGRN model can automatically perform an interpretable reasoning process over a general dependency

parse tree from the question, which can largely broaden its application fields. The attention module encourages the model to attend the local visual evidence, while the gated residual composition module can learn to compose and update the knowledge from its child nodes, and the parse-tree-guided propagation module generates and propagates the edge-dependent information from children to their parents. Experiments show that our PTGRN outperforms previous neural network models without using any specified ground-truth layouts or complicated handcrafted rules.

## REFERENCES

- [1] M. Malinowski, M. Rohrbach, and M. Fritz, “Ask your neurons: A neural-based approach to answering questions about images,” in *ICCV*, 2015, pp. 1–9.
- [2] J. Lu, J. Yang, D. Batra, and D. Parikh, “Hierarchical question-image co-attention for visual question answering,” in *NIPS*, 2016, pp. 289–297.
- [3] J.-H. Kim, K. W. On, J. Kim, J. Ha, and B.-T. Zhang, “Hadamard product for low-rank bilinear pooling,” *CoRR*, vol. abs/1610.04325, 2016.
- [4] Y. Goyal, T. Khot, D. Summers-Stay, D. Batra, and D. Parikh, “Making the V in VQA matter: Elevating the role of image understanding in Visual Question Answering,” in *CVPR*, 2017.
- [5] J. Johnson, B. Hariharan, L. van der Maaten, L. Fei-Fei, C. L. Zitnick, and R. Girshick, “CLEVR: A diagnostic dataset for compositional language and elementary visual reasoning,” in *CVPR*, 2017.
- [6] R. Hu, J. Andreas, M. Rohrbach, T. Darrell, and K. Saenko, “Learning to reason: End-to-end module networks for visual question answering,” in *ICCV*, 2017.
- [7] J. Johnson, B. Hariharan, L. van der Maaten, J. Hoffman, F. Li, C. L. Zitnick, and R. B. Girshick, “Inferring and executing programs for visual reasoning,” in *ICCV*, 2017.
- [8] D. Teney, L. Liu, and A. van den Hengel, “Graph-structured representations for visual question answering,” in *CVPR*, July 2017.
- [9] S. Antol, A. Agrawal, J. Lu, M. Mitchell, D. Batra, C. L. Zitnick, and D. Parikh, “VQA: Visual Question Answering,” in *ICCV*, 2015.
- [10] I. Ilievski, S. Yan, and J. Feng, “A focused dynamic attention model for visual question answering,” *CoRR*, vol. abs/1604.01485, 2016.
- [11] H. Xu and K. Saenko, *Ask, Attend and Answer: Exploring Question-Guided Spatial Attention for Visual Question Answering*. Cham: Springer International Publishing, 2016, pp. 451–466.
- [12] K. J. Shih, S. Singh, and D. Hoiem, “Where to look: Focus regions for visual question answering,” in *CVPR*, 2016.
- [13] Y. Zhu, O. Groth, M. S. Bernstein, and L. Fei-Fei, “Visual7w: Grounded question answering in images,” in *CVPR*, 2016, pp. 4995–5004.
- [14] Z. Yang, X. He, J. Gao, L. Deng, and A. Smola, “Stacked attention networks for image question answering,” in *CVPR*, June 2016, pp. 21–29.
- [15] A. Fukui, D. H. Park, D. Yang, A. Rohrbach, T. Darrell, and M. Rohrbach, “Multimodal compact bilinear pooling for visual question answering and visual grounding,” in *EMNLP*, 2016, pp. 457–468.
- [16] Z. Yu, J. Yu, J. Fan, and D. Tao, “Multi-modal factorized bilinear pooling with co-attention learning for visual question answering,” *IEEE International Conference on Computer Vision (ICCV)*, pp. 1839–1848, 2017.
- [17] H. Ben-younes, R. Cadene, M. Cord, and N. Thome, “Mutan: Multimodal tucker fusion for visual question answering,” in *ICCV*, Oct 2017.
- [18] A. Jabri, A. Joulin, and L. van der Maaten, “Revisiting visual question answering baselines,” in *ECCV*, ser. Lecture Notes in Computer Science, vol. 9912. Springer, 2016, pp. 727–739.
- [19] A. Kumar, O. Irsoy, P. Ondruska, M. Iyyer, J. Bradbury, I. Gulrajani, V. Zhong, R. Paulus, and R. Socher, “Ask me anything: Dynamic memory networks for natural language processing,” in *ICML*, 2016, pp. 1378–1387.
- [20] P. Wang, Q. Wu, C. Shen, A. van den Hengel, and A. R. Dick, “FVQA: fact-based visual question answering,” *CoRR*, vol. abs/1606.05433, 2016.



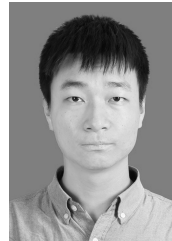
- [21] Y. Zhu, J. J. Lim, and L. Fei-Fei, "Knowledge Acquisition for Visual Question Answering via Iterative Querying," in *CVPR*, 2017.
- [22] C. Xiong, S. Merity, and R. Socher, "Dynamic memory networks for visual and textual question answering," in *ICML*, 2016, pp. 2397–2406.
- [23] J. Andreas, M. Rohrbach, T. Darrell, and D. Klein, "Neural module networks," in *CVPR*. IEEE Computer Society, 2016, pp. 39–48.
- [24] —, "Learning to compose neural networks for question answering," in *HLT-NAACL*. The Association for Computational Linguistics, 2016, pp. 1545–1554.
- [25] V. S. Lempitsky and A. Zisserman, "Learning to count objects in images," in *NIPS*. Curran Associates, Inc., 2010, pp. 1324–1332.
- [26] C. Zhang, H. Li, X. Wang, and X. Yang, "Cross-scene crowd counting via deep convolutional neural networks," in *CVPR*. IEEE Computer Society, 2015, pp. 833–841.
- [27] D. Oñoro-Rubio and R. J. López-Sastre, "Towards perspective-free object counting with deep learning," in *ECCV (7)*, ser. Lecture Notes in Computer Science, vol. 9911. Springer, 2016, pp. 615–629.
- [28] J. Zhang, S. Ma, M. Sameki, S. Sclaroff, M. Betke, Z. Lin, X. Shen, B. L. Price, and R. Mech, "Salient object subitizing," *International Journal of Computer Vision*, vol. 124, no. 2, pp. 169–186, 2017.
- [29] P. Chattopadhyay, R. Vedantam, R. R. Selvaraju, D. Batra, and D. Parikh, "Counting everyday objects in everyday scenes," in *CVPR*. IEEE Computer Society, 2017, pp. 4428–4437.
- [30] P. Anderson, X. He, C. Buehler, D. Teney, M. Johnson, S. Gould, and L. Zhang, "Bottom-up and top-down attention for image captioning and visual question answering," *arXiv preprint arXiv:1707.07998*, 2017.
- [31] R. Krishna, Y. Zhu, O. Groth, J. Johnson, K. Hata, J. Kravitz, S. Chen, Y. Kalantidis, L.-J. Li, D. A. Shamma, M. S. Bernstein, and L. Fei-Fei, "Visual genome: Connecting language and vision using crowdsourced dense image annotations," *International Journal of Computer Vision*, vol. 123, no. 1, pp. 32–73, May 2017. [Online]. Available: <https://doi.org/10.1007/s11263-016-0981-7>
- [32] A. Trott, C. Xiong, and R. Socher, "Interpretable counting for visual question answering," *CoRR*, vol. abs/1712.08697, 2017.
- [33] Y. Zhang, J. Hare, and A. Prützel-Bennett, "Learning to count objects in natural images for visual question answering," in *International Conference on Learning Representations*, 2018.
- [34] D. Chen and C. D. Manning, "A fast and accurate dependency parser using neural networks," in *EMNLP*, 2014.
- [35] K. He, X. Zhang, S. Ren, and J. Sun, "Deep residual learning for image recognition," in *CVPR*. IEEE Computer Society, 2016, pp. 770–778.
- [36] J. Chung, Ç. Gülçehre, K. Cho, and Y. Bengio, "Empirical evaluation of gated recurrent neural networks on sequence modeling," *CoRR*, vol. abs/1412.3555, 2014.
- [37] K. S. Tai, R. Socher, and C. D. Manning, "Improved semantic representations from tree-structured long short-term memory networks," in *ACL (1)*. The Association for Computer Linguistics, 2015, pp. 1556–1566.
- [38] M. de Marneffe, T. Dozat, N. Silveira, K. Haverinen, F. Ginter, J. Nivre, and C. D. Manning, "Universal stanford dependencies: A cross-linguistic typology," in *LREC*. ELRA, 2014, pp. 4585–4592.
- [39] S. E. Kahou, A. Atkinson, V. Michalski, Á. Kádár, A. Trischler, and Y. Bengio, "Figureqa: An annotated figure dataset for visual reasoning," *CoRR*, vol. abs/1710.07300, 2017.
- [40] A. Santoro, D. Raposo, D. G. T. Barrett, M. Malinowski, R. Pascanu, P. Battaglia, and T. P. Lillicrap, "A simple neural network module for relational reasoning," *CoRR*, vol. abs/1706.01427, 2017.
- [41] C. Zhu, Y. Zhao, S. Huang, K. Tu, and Y. Ma, "Structured attentions for visual question answering," in *ICCV*, Oct 2017.
- [42] M. Schuster and K. Paliwal, "Bidirectional recurrent neural networks," *Trans. Sig. Proc.*, vol. 45, no. 11, pp. 2673–2681, Nov. 1997.
- [43] D. P. Kingma and J. Ba, "Adam: A method for stochastic optimization," in *ICLR*, 2015.
- [44] E. Perez, F. Strub, H. de Vries, V. Dumoulin, and A. C. Courville, "Film: Visual reasoning with a general conditioning layer," in *AAAI*. AAAI Press, 2018.



**Qingxing Cao** Qingxing Cao received his B.S. degree in software engineering from Sun Yat-Sen University, Guangzhou, China, in 2013. He is currently pursuing his Ph.D. degree in computer science and technology at Sun Yat-Sen University, advised by Professor Liang Lin. His current research interests include computer vision.



**Xiaodan Liang** Xiaodan Liang is currently an Associate Professor at Sun Yat-sen University. She was a postdoc researcher in the Machine Learning Department at Carnegie Mellon University, working with Prof. Eric Xing, from 2016 to 2018. She received her PhD degree from Sun Yat-sen University in 2016, advised by Liang Lin. She has published several cutting-edge projects on human-related analysis, including human parsing, pedestrian detection and instance segmentation, 2D/3D human pose estimation and activity recognition.



**Bailin Li** Bailin Li received his B.E. degree from Jilin University, Changchun, China, in 2016, and is currently working toward his M.S. degree at the School of Electronics and Information Technology (School of Microelectronics), Sun Yat-Sen University, Guangzhou, China. His research interests include computer vision and machine learning.



**Liang Lin** Liang Lin (M09, SM15) is the Executive R&D Director of SenseTime Group Limited and a full Professor of Sun Yat-sen University. From 2008 to 2010, he was a Post-Doctoral Fellow at University of California, Los Angeles. From 2014 to 2015, as a senior visiting scholar, he was with The Hong Kong Polytechnic University and The Chinese University of Hong Kong. He currently leads the SenseTime R&D teams to develop cutting-edge and deliverable solutions on computer vision, data analysis and mining, and intelligent robotic systems. He has authored and co-authored more than 100 papers in top-tier academic journals and conferences. He has been serving as an associate editor of IEEE Trans. Human-Machine Systems, The Visual Computer and Neurocomputing. He has served as area/session chairs for numerous conferences, such as ICME, ACCV, ICMR. He was the recipient of Best Paper Runners-Up Award in ACM NPAR 2010, Google Faculty Award in 2012, Best Paper Diamond Award in IEEE ICME 2017, and Hong Kong Scholars Award in 2014. He has been supported by several promotive funds for his research works such as Excellent Young Scientist of the National Natural Science Foundation of China. He is a Fellow of IET.